5分振動から探る太陽内部回転構造

HDSセミナー

2005年6月9日

安藤裕康

内部回転構造はなぜ重要か

太陽周期11年（22年）は何が引き起こしているか
　ダイナモは何がどこで起っているか
　　グローバルな子午環流が必要
　　表面対流層の底で磁場が発生
　　それ以外は？

5分振動の観測史
1970年代

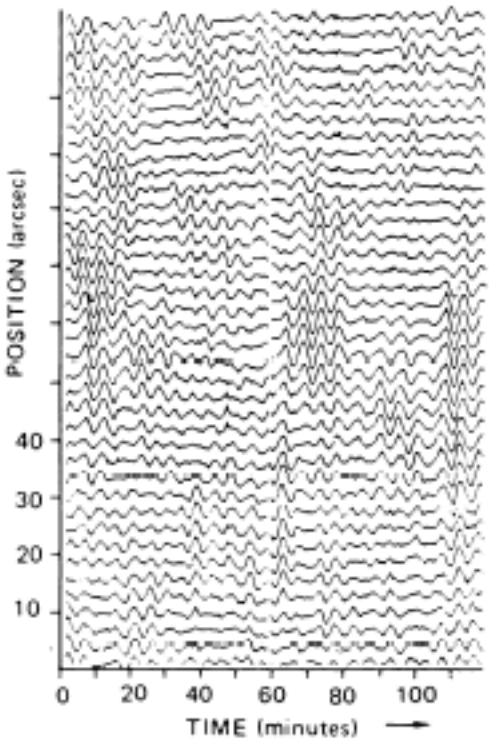

Figure 2. Doppler velocity as a function of time and position on the solar disk. The separation between adjacent curves corresponds to a velocity amplitude of $400\,\mathrm{m\,s^{-1}}$. *(Adapted from Musman & Rust 1970.)*

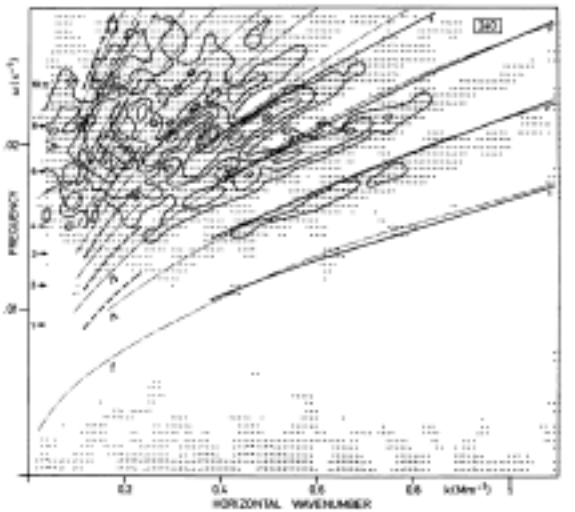

Figure 3. Observed power spectrum of the solar five-minute oscillations (Deubner 1975). The hatching and contours show power as a function of horizontal wavenumber k_h *and angular frequency* ω, *from four hours of observations extending over approximately half the solar diameter. The solid, dashed and dot-dashed lines show frequencies computed by Ulrich (1970), Wolff (1972) and Ando & Osaki (1975), respectively.*

3. HIGH-DEGREE MODES OF THE SOLAR INTERIOR

観測の高精度化（グローバルモード、連続観測）
1980年代

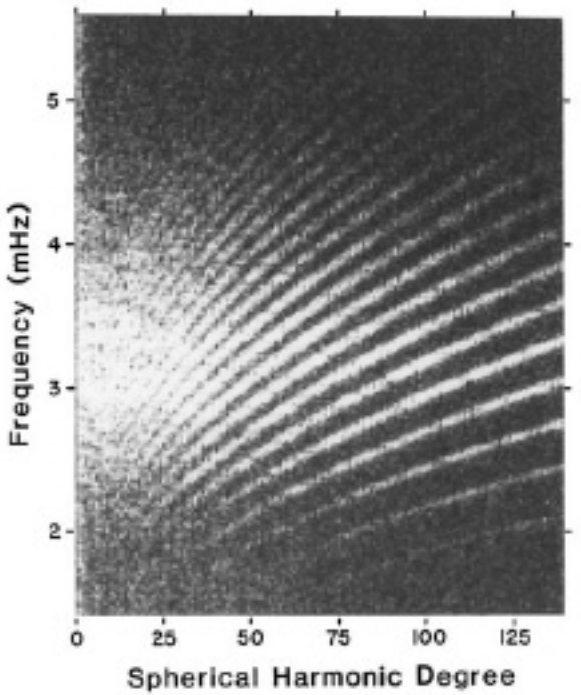

Figure 12. Spectrum of solar oscillations of degree up to around 140, obtained from four days of Doppler observations on a solar image optically collapsed in the direction orthogonal to the rotation axis. The frequency resolution has been degraded to 8 μHz. (From Duvall & Harvey 1983.)

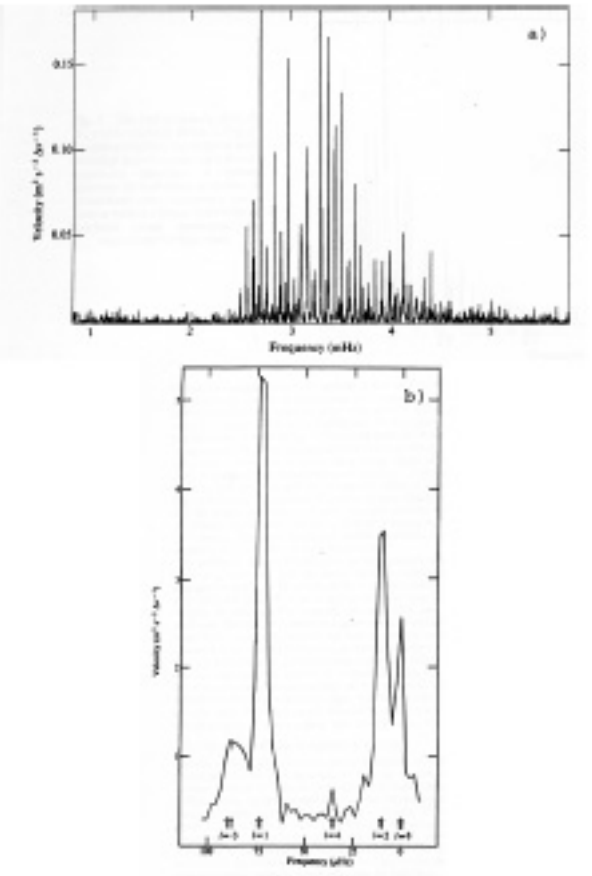

Figure 10. (a) Power spectrum of continuous 5-day whole-disk Doppler velocity observation from the South Pole. (b) Superposition of segments of length 136 μHz from the spectrum shown in panel a). (From Grec et al. 1980.)

荒い回転構造

回転による振動数のシフト量を測定

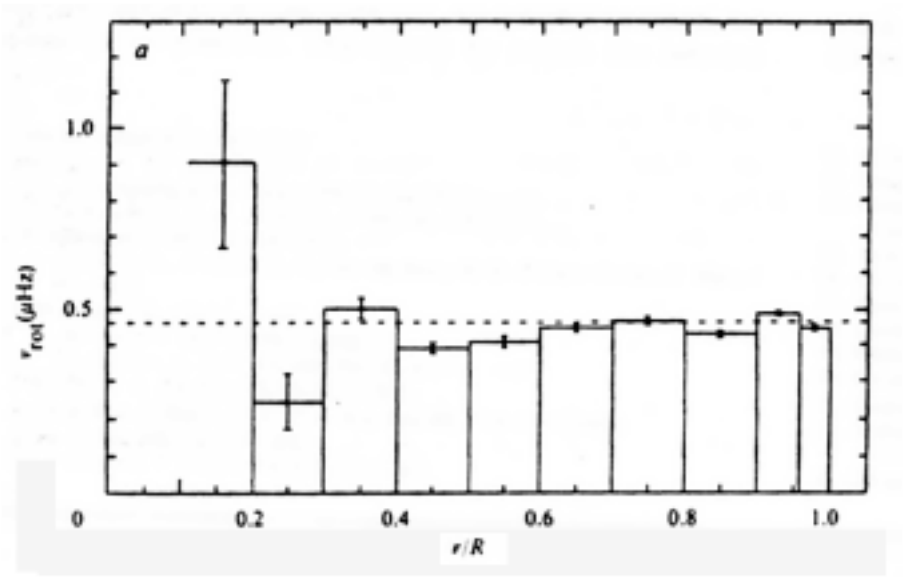

Figure 14. Inferred solar equatorial rotation rate, from observations by Duvall & Harvey (1984) of sectoral-mode rotational splittings, as a function of fractional radius r/R. A piece-wise constant solution has been fitted, in a least-squares sense, to the observed splittings. The average error bars reflect the observational uncertainties. The dashed line shows the surface equatorial rotation rate. (From Duvall et al. 1984.)

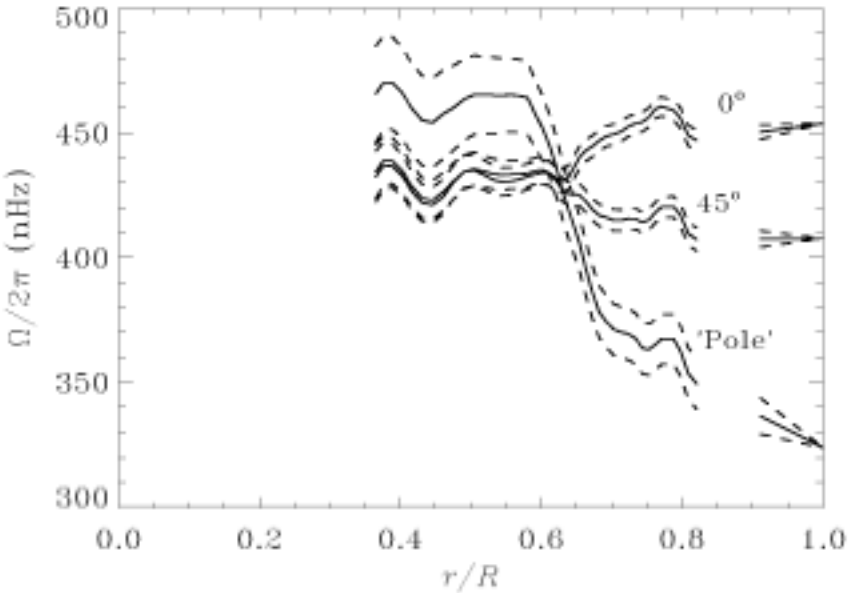

Figure 16. Rotation rate inferred from inversion of the rotational splittings of Libbrecht (1988b, 1989); the dashed lines indicate the $1-\sigma$ error limits. The surface values are indicated by the straight lines starting at $r/R = 1$. Note that the results indicated at the 'Pole' in fact correspond to an extrapolation from lower latitudes. (Adapted from Christensen-Dalsgaard & Schou 1988.)

5分振動の観測プロジェクト

1. GONG(Global Oscillation Network Group)
   since 1995

2. MDI(Michelson Doppler Imager on SOHO
   since 1996

回転の定義

$$A(h,t) = \int_h^{R_\odot} J(r,t)\, dr \qquad (1)$$

with

$$J(r,t) = 2\pi\, \rho r^4 \int_0^{\pi} \Omega(r,\theta,t)\, \sin^3\theta\, d\theta\,, \qquad (2)$$

$$\bar{\Omega}(r,t) = \tfrac{3}{4} \int_0^{\pi} \Omega(r,\theta,t)\, \sin^3\theta\, d\theta\,. \qquad (3)$$

The angular momentum, $A(h,t)$, can then be written as

$$A(h,t) = \frac{8\pi}{3} \int_h^{R_\odot} \rho r^4\, \bar{\Omega}(r,t)\, dr\,. \qquad (4)$$

We also define the solid-body rotation of the Sun, Ω_0, for the region $(R_l, R_\odot)$ where R_l is the smallest value of h in our analysis,

$$\Omega_0(t) \int_{R_l}^{R_\odot} \rho r^4\, dr = \int_{R_l}^{R_\odot} \rho r^4\, \bar{\Omega}(r,t)\, dr\,. \qquad (5)$$

精密な観測

1990年代

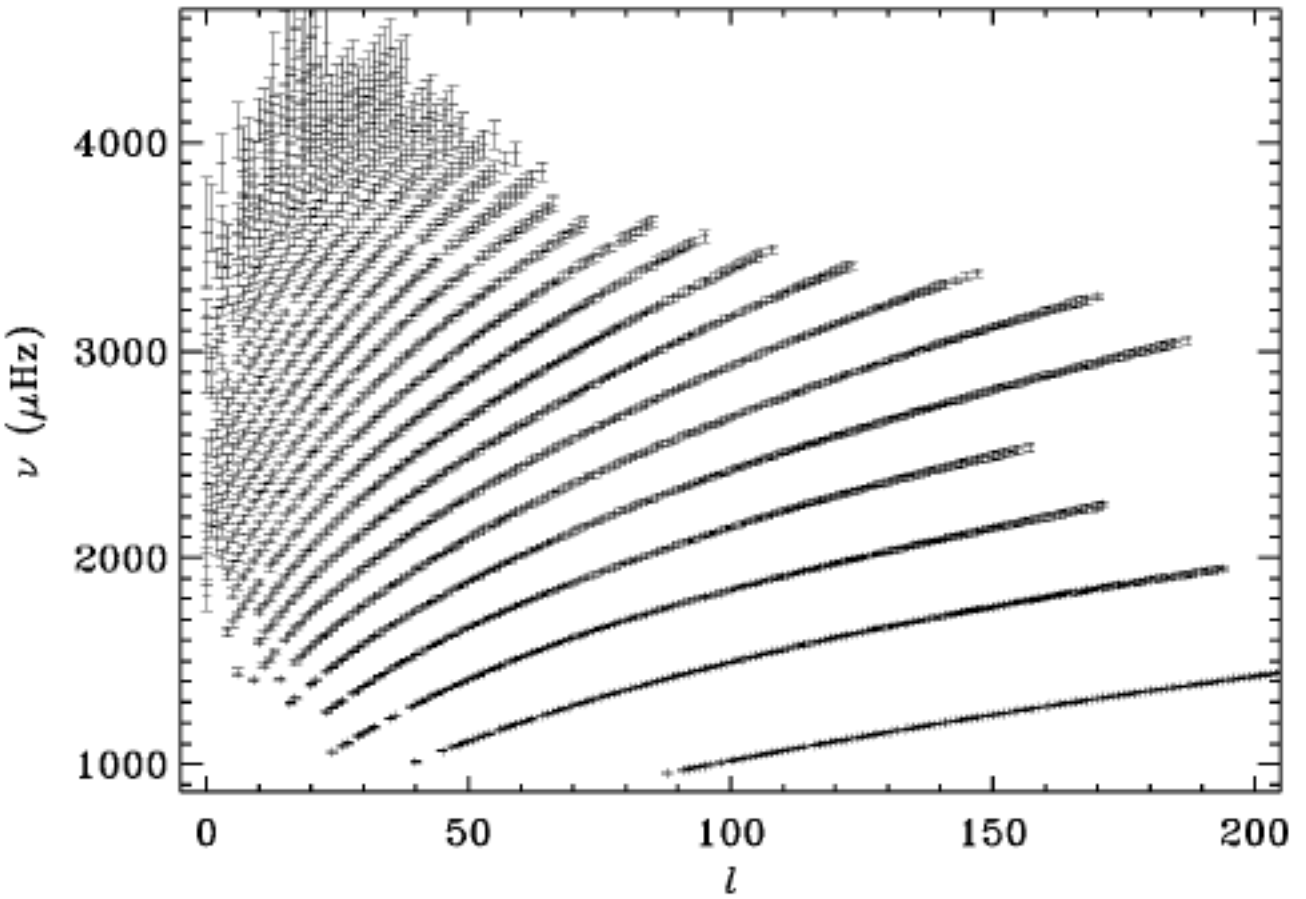

Figure 17. Observed multiplet frequencies from 144 days of MDI observations, against degree l; the error bars correspond to 1000σ. The lowest set of modes are the f modes. (See Schou et al. 1998.)

5分振動解析による内部回転のグローバル構造

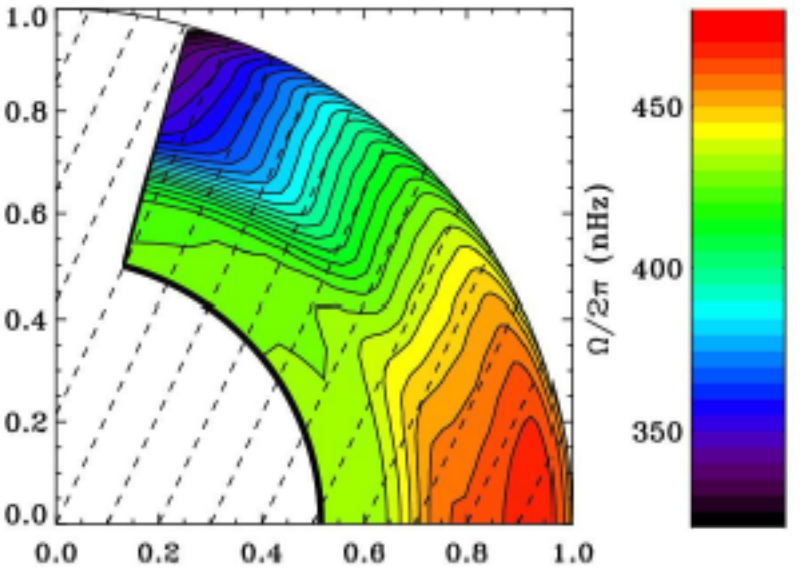

Figure 1. Mean rotation profile for RLS inversions of GONG data. The dashed lines make a 25° angle to the rotation axis.

Figure 20. *izontal axis and the rotation axis along the vertical axis. Selected contours have been labelled by the rotation rate. The dashed circle marks the base of the convection zone, and the tick marks along the outer circle are at latitudes 15°, 30°, 45°, 60° and 75°. The analysis used OLA inversion of 144 days of MDI data. The black area shows a part of the Sun for which no reliable determination is possible with this data set. (Adapted from Schou et al. 1998.)*

これを再現する回転理論はまだ無い

内部回転の動径構造

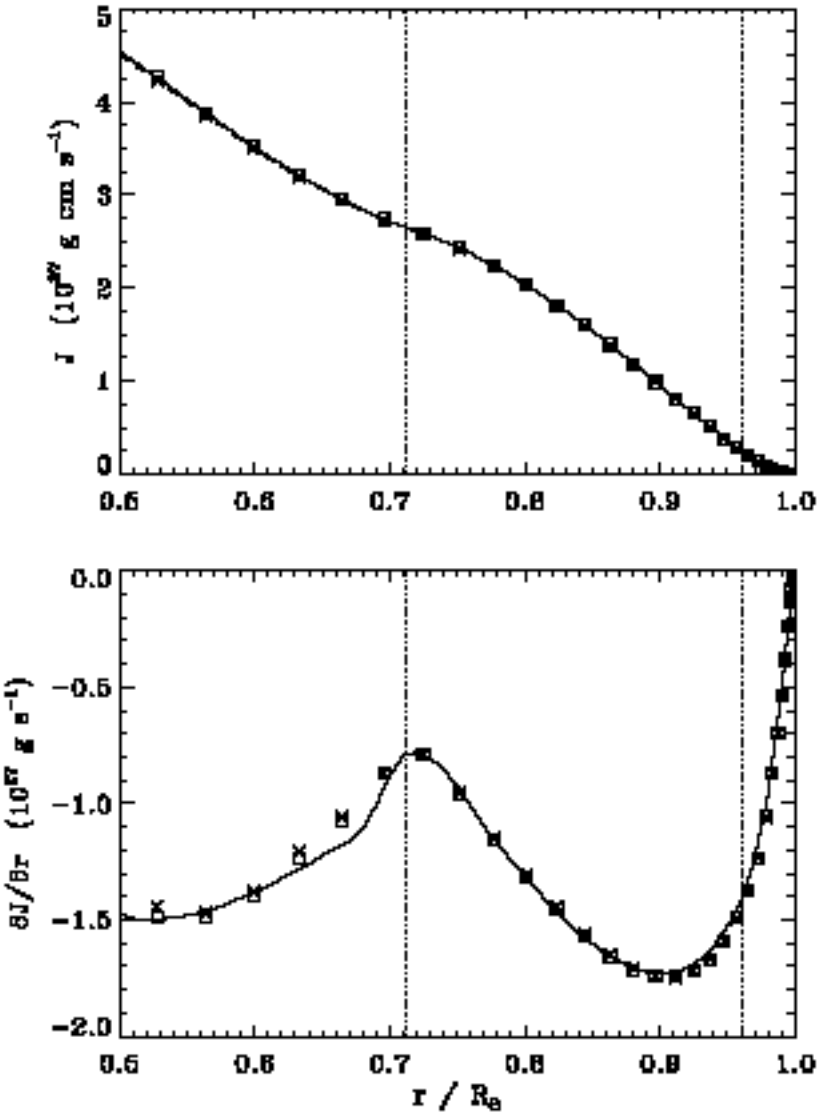

FIG. 1.—*Top:* Angular momentum of a thin spherical shell divided by its depth, J, as a function of radius averaged over all data sets. *Crosses, solid line*: GONG data. *Squares, dashed line*: MDI data. *Bottom:* Radial gradient of J (*symbols*) and the radial gradient of $\rho \times r^4$ (*solid line*). *Vertical dotted lines*: Upper shear layer at $r = 0.96\ R_\odot$ and the base of the convection zone at $r = 0.71\ R_\odot$.

内部回転の (r-θ) 構造

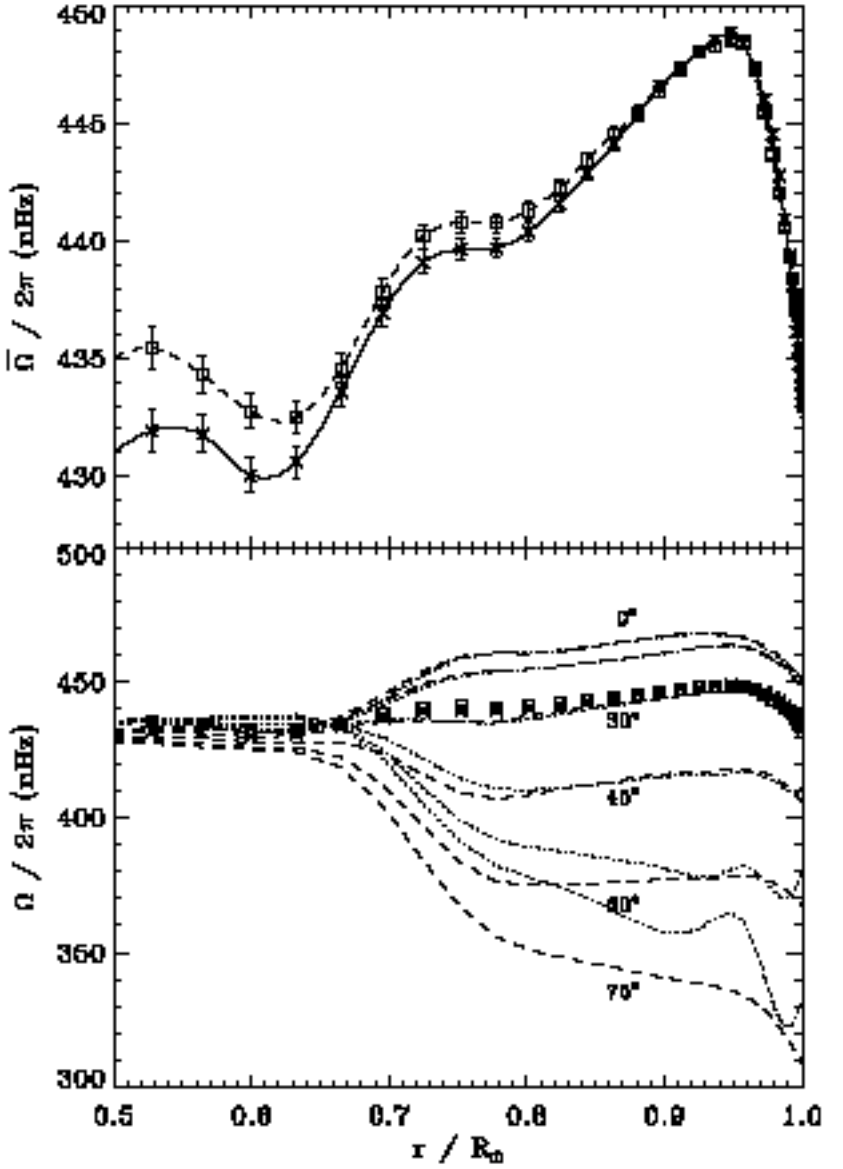

FIG. 2.—*Top:* Corresponding θ-independent angular velocity, $\bar{\Omega}$, averaged over all data sets as a function of radius. *Bottom:* Average rotation rate Ω at 0°, 15°, 30°, 45°, 60°, and 75° from GONG (*dashed lines*) and MDI data (*dotted lines*) compared to $\bar{\Omega}$. *Crosses*: GONG data. *Squares*: MDI data.

表面の速度場の時間変化

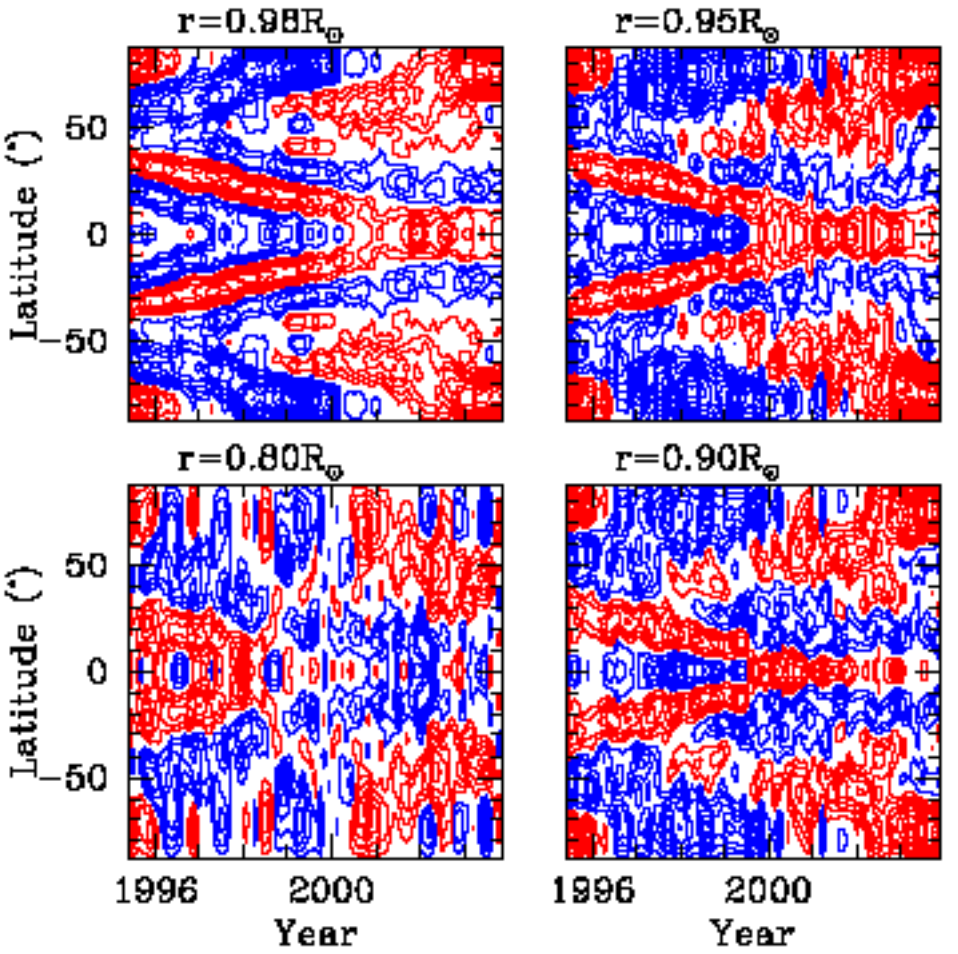

Figure 1. A contour diagram of the rotation-velocity residuals obtained using 2D RLS inversion of GONG data shown at a few representative depths. The red contours are for positive δv_ϕ, while blue contours denote negative values. The contours are drawn at intervals of 1 m/s; the contour for zero velocity is not shown.

内部回転の時間変化

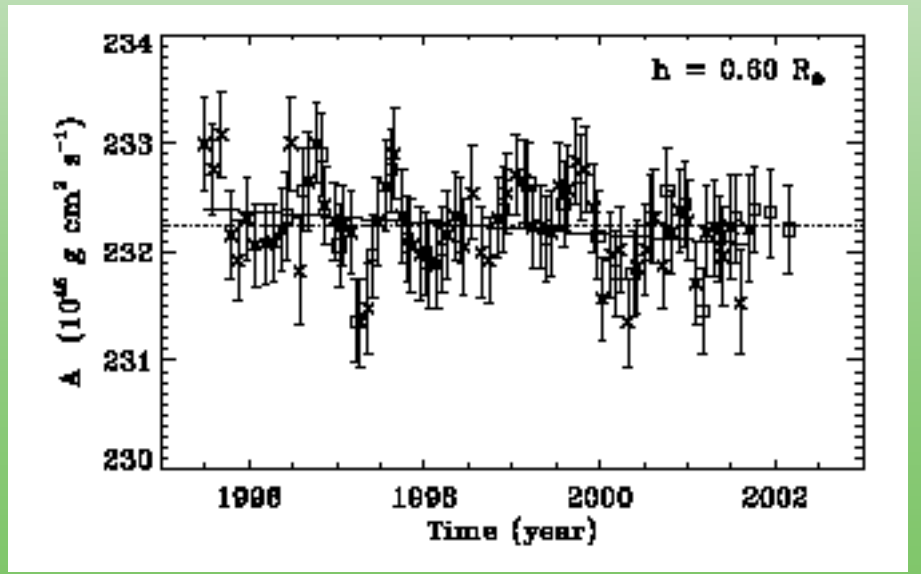

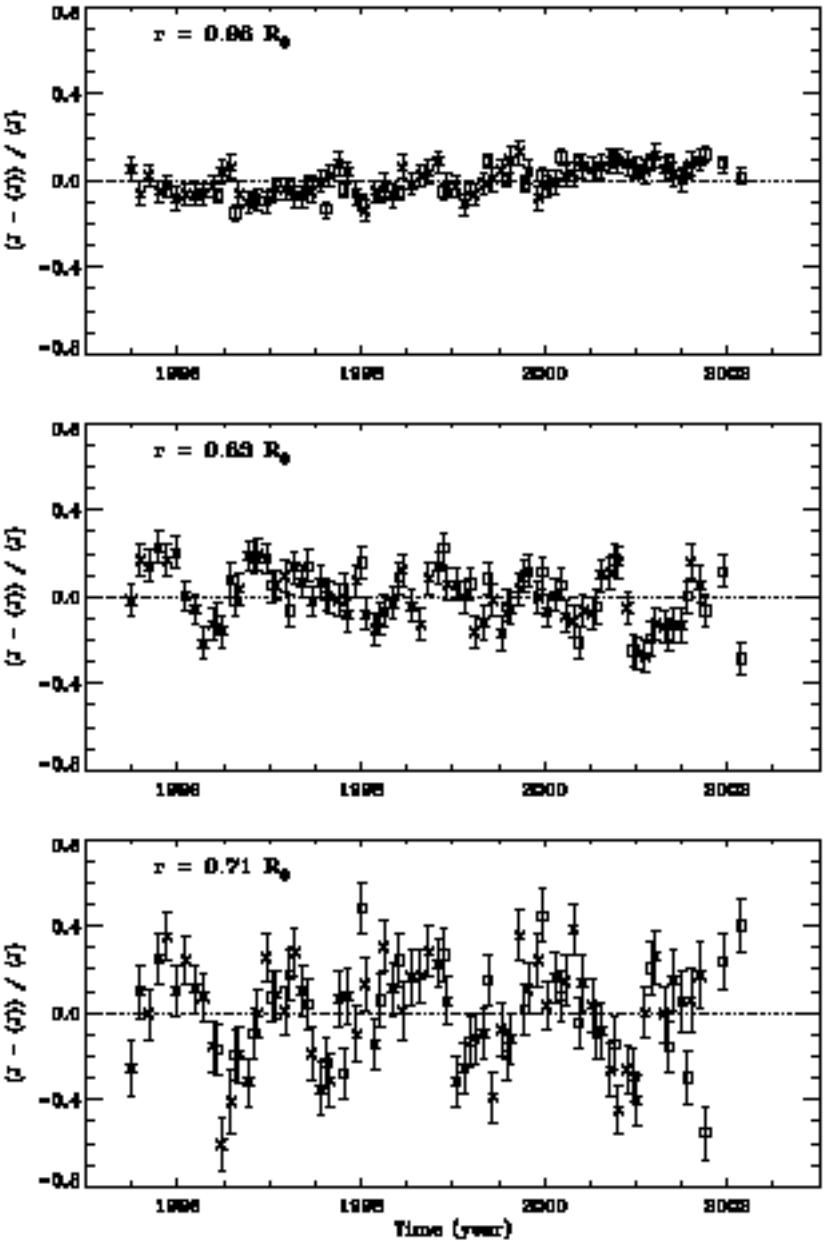

FIG. 4.—Residual angular momentum (percentages), the difference between J and its temporal average divided by the average, at three locations in the convection zone derived from GONG (*crosses*) and MDI data (*squares*).

波動と回転の相互作用

g-mode（内部重力波）と回転との相互作用

1 Kummar et al 1999

2 Kim and MacGregor 2001

Kim & MacGregor の結果

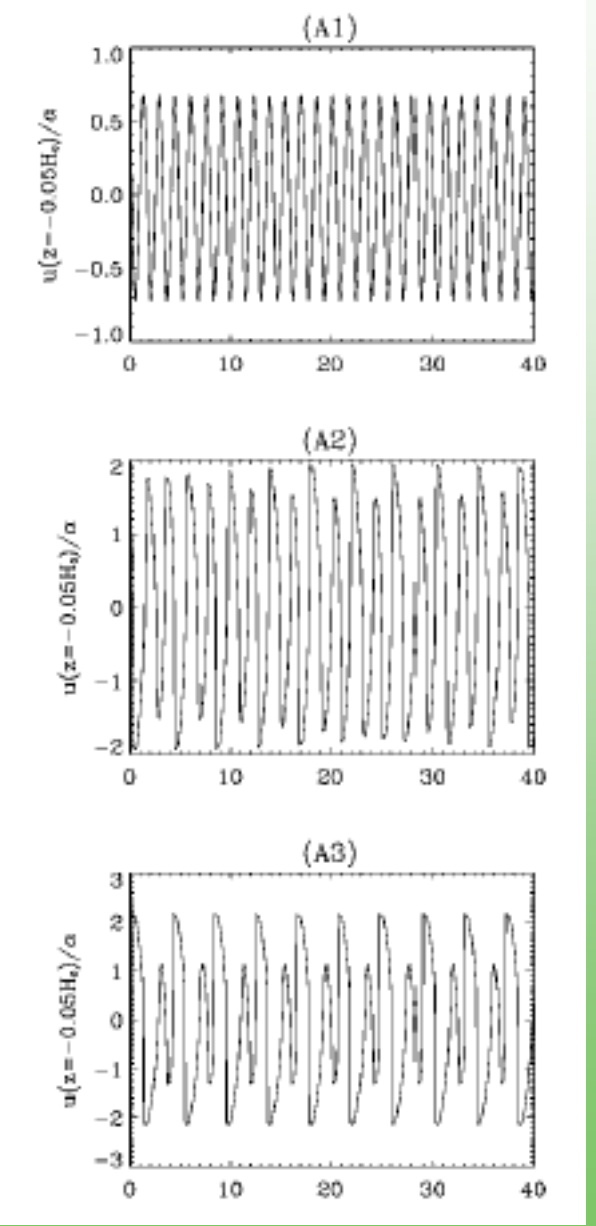

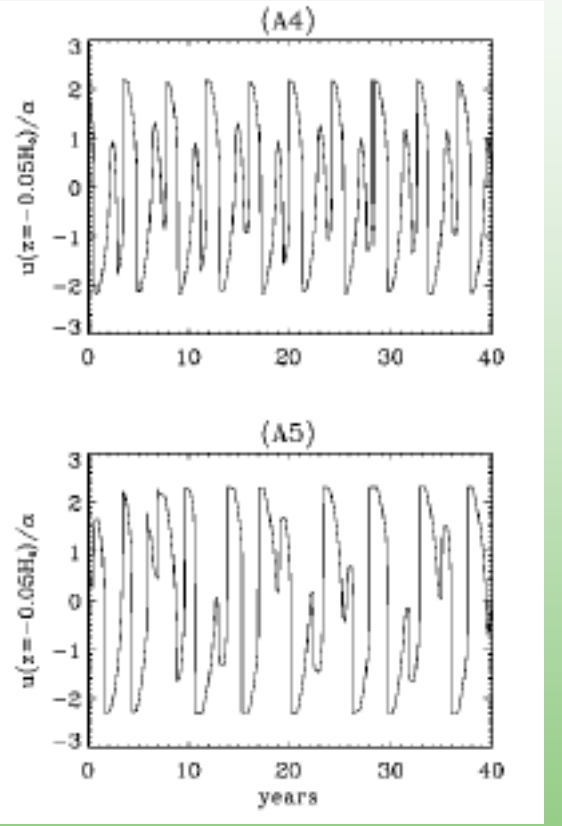

Be星における質量放出現象と波動

・恒星赤道周辺からの準周期的質量放出
　数ヶ月〜100年（もっと長い？）

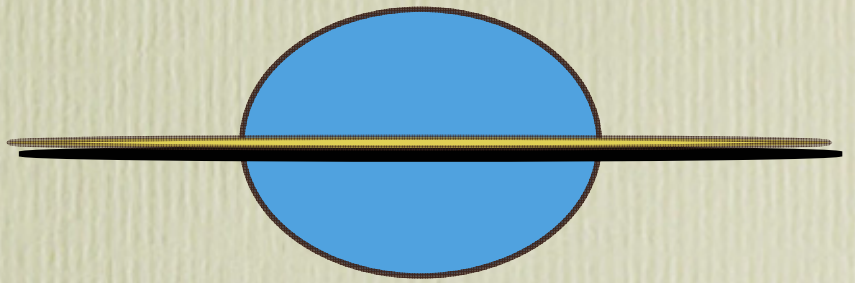

・波動（非動径振動; i.e., NRP）の存在
　1970後半〜1980年代　CCDの登場で明確に

Walker et al(1979), Baade(1979), Bolton(1982),
Vogt & Penrod(1983)

NRPの衝撃波による質量放出

Vogt & Penrod (1983)

NRPによる角運動量の再配分

・波動による角運動量の再配分と質量放出（作業仮説）

Ando(1982)

・波動による角運動量再配分の定量的見積もり

Ando(1983)

・NRPのPrograde modeによる回転速度の加速と質量放出

Osaki(1986)

波動と回転の相互作用の具体的提案　Ando(1986)

要請

・ProgradeとRetrogradeのモードが同時に存在
（κ ーMechanismのような励起機構要請）

・基本方程式

$$\frac{\partial u}{\partial t} = -\frac{1}{2}\sum_{j=1}^{n}\left[m\delta_T PIm\left\{\left(\frac{\delta P}{P}\right)^* s\right\}\right]_j + \nu\,\Delta u,$$

$$\frac{\partial \hat{u}}{\partial \hat{t}} = m^2 F_1\left(\hat{u} - Q\int_0^x F_2\hat{u}\,dx\right)\exp\left\{-\int_0^x E\,dx\right\}|Y_l^m|^2 + \Lambda\,\Delta\hat{u},$$

安定性：　$F_1 > 0$　不安定　（早期型星）
$F_1 < 0$　安定　（晩期型星）

計算結果

・準周期的な加速と減速が起こる
　　範囲は波動の位相速度は越えない

・加速領域ではPrograde modeのシールディングが、
減速領域ではRetrograde modeのシールディングが
それぞれ起こる

・変化の準周期を決めているもの
波動のエネルギー、
輻射損失の時間≈波動の周期　が成り立つ場所の深さ

with (A) $\omega_0 = 0.3$, $V_0 = 1\,\mathrm{km\,s^{-1}}$, and $\hat{T} = 0.06$, and (B) $\omega_0 = 0.1$, $V_0 = 1\,\mathrm{km\,s^{-1}}$, and $\hat{T} = 4$, the oscillation period T is

$$T \sim \frac{7.2}{m^2}\ \mathrm{yr\ (case\ A)}.$$

$$\sim \frac{53}{m^2}\ \mathrm{yr\ (case\ B)}.$$

$$T = \frac{4\pi}{m^2 a_0^2}\sqrt{R^3/GM}\,\hat{T} = \frac{4\pi\omega_0^2}{m^2 V_0^2}\sqrt{GMR}\,\hat{T}, \qquad (13)$$

20M ZAMS
2つのg-mode

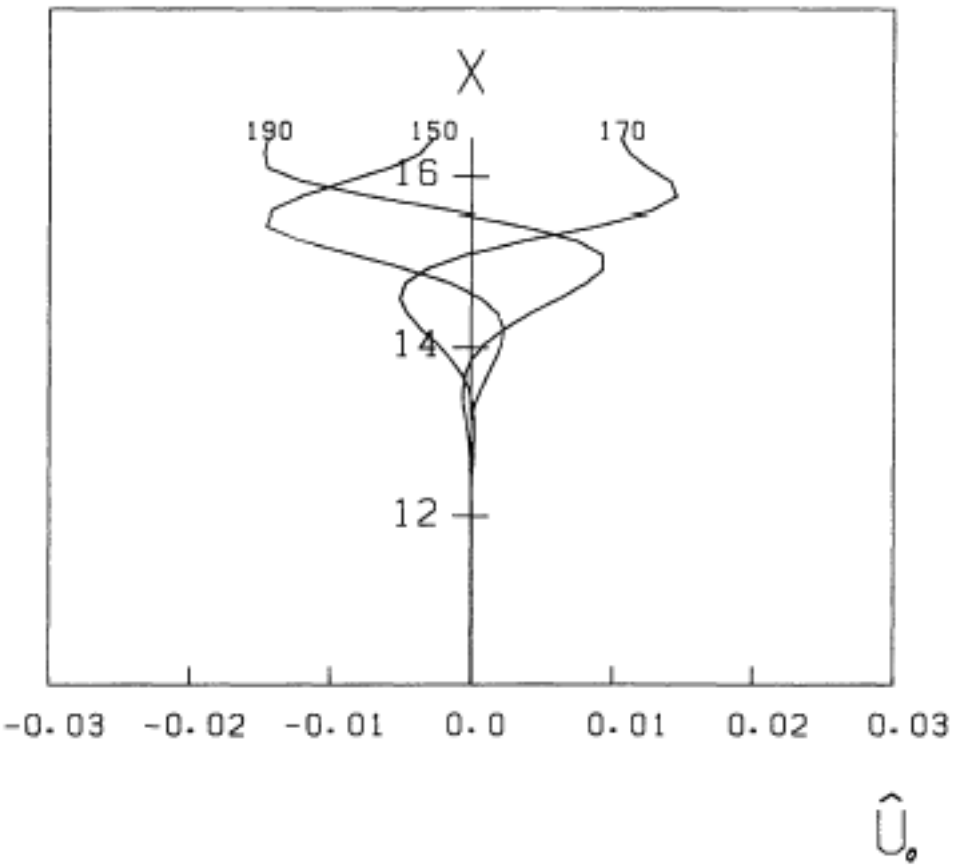

Fig. 3. The nonlinear calculation of the oscillation of rotation profile for the same model as in Fig. 2. The full scale of the abscissa is given by the phase speed (ω_0/m). In the subsequent figures, this convention is also used

共通の物理機構

波動と回転の相互作用

太陽の対流層

1．3年周期の時間変動活動と11（22）年周期活動との結びつき

Be星の赤道からの質量放出

具体的な赤道円盤の形成